Journal of

Materials Chemistry A

PAPER

Phosphine-Oxide Modulator Ameliorates Hole Injection for Blue Perovskite Light-Emitting Diodes

Received 00th January 20xx,
Accepted 00th January 20xx

DOI: 10.1039/x0xx00000x

Xiangyang Fan,[a] Yu Wang,[b] Xinyu Shen,*[c,d] Zhongkai Yu,[a] Woo Hyeon Jeong,[c] Ji Won Jang,[e] Yeong Gyeong Kim,[a] Seung-Je Woo,[f] Hyungju Ahn,[g] Hyosung Choi,[e] Tae-Woo Lee,[f] Sung Heum Park,[a] Feng Gao,[b] and Bo Ram Lee*[c]

Incongruously with enormous developments in perovskite light-emitting diodes (PeLEDs) recently, efficient blue PeLEDs have widely been considered a critical challenge due to the non-radiative recombination and unbalanced charge injection caused by the unmatched carrier mobility and the deep hole injection barrier between the hole transport layer (HTL) and emissive layer (EML). Here, we incorporate tris(4-trifluoromethylphenyl)phosphine-oxide (TMFPPO) obtained through a facile oxidation synthesis process into poly(9-vinylcarbazole) (PVK). TMFPPO incorporation modulates the energy level and hole mobility of the binary-blend HTLs to eliminate the hole injection barrier and balance charge injection within EML. Consequently, the blue PeLEDs with blended HTL present an external quantum efficiency (EQE) of 7.23% centred 477 nm, much higher than the EQE of a PVK device (4.95%). Our results demonstrate that modulating the energy level as well as the charge injection of the HTL in the device is a promising method for obtaining efficient blue PeLEDs.

Introduction

Metal halide perovskites have attracted enormous attention owing to their unique optical properties, such as impressive broad colour gamut, high colour purity, and photoluminescence quantum yields (PLQYs).[1-5] These merits emphasize the potential applications of perovskite light-emitting diodes (PeLEDs) in next-generation display and illumination.[6-12] Despite the considerable advances in enhancing the external quantum efficiencies (EQEs) of green (30.84%), red (25.8%), and near-infrared (23.8%) PeLEDs,[13-19] the current highest EQE of blue PeLEDs (~480 nm) is only 18.65%,[20] lagging far behind those of narrow bandgap PeLEDs and slowing the path to their application in full-colour displays.[21-27] Among the perovskite family members, quasi-two dimensional (2D) perovskites exhibit a desirable film morphology with low roughness and high coverage, as well as enhanced radiative recombination rates benefiting from strong charge carrier confinement and large exciton binding energies, making them highly efficient materials for blue PeLEDs.[28-30] However, the quasi-2D blue PeLEDs are suffering from imbalanced charge injection due to unmatched carrier mobility and large hole injection barrier between the highest occupied molecular orbital (HOMO) levels of hole transport layer (HTL) and perovskite emissive layer (EML). These induce charge accumulation at the interface, nonradiative recombination, Joule heating and device degradation under bias voltage,[31-33] ultimately causing a decrease in operational lifetime and spectral stability.[34, 35]

Various strategies to balance the charge injection of quasi-2D blue PeLEDs have been explored, including interface modification and device architecture optimization. For example, Choy et al. introduced a thin layer of poly(sodium-4-styrene sulfonate) on NiOx to form a bilayer HTL structure to deep the HOMO level and boost the hole injection of quasi-2D blue PeLEDs, leading to an EQE of 1.45%.[36] Drawing on the experience of green PeLEDs, perfluorinated ionomer (PFI) has been used to dope poly (3,4-ethylenedioxythiophene) : poly (styrenesulfonic acid) (PEDOT:PSS) or modify poly (9-vinylcarbazole) (PVK) to reduce the hole injection barrier of blue PeLEDs.[37, 38] The HOMO of PEDOT:PSS can be modulated from -5.05 to -5.30 eV with L-phenylalanine, leading to a peak EQE of 10.98% at 480 nm.[39] In our previous work, 2-(4-biphenyl)-5-(4-t-butyl-phenyl)-1,3,4-oxadiazole with HOMO at -6.2 eV was blended to PVK to boost the hole injection, leading to an EQE of 4.53% .[40] However, there are still hole injection barriers from the HTL to perovskite EML in these works.

In this study, inspired by the deep HOMO level of phosphine oxide derivatives exhibited in phosphorescent organic LEDs,[41-43] we developed tris(4-trifluoromethylphenyl)phosphine-oxide (TMFPPO) with a deep HOMO level (-6.46 eV) by oxidizing tris(4-trifluoromethylphenyl)phosphine (TMFPP). The presence of highly electronegative fluorine is not only important for achieving a deep HOMO level, but also improves the thermal stability of the HTL.[44-46]

[a] Department of Physics, Pukyong National University, and CECS Research Institute, Core Research Institute, Busan 48513, Republic of Korea
[b] Biomolecular and organic electronics, Department of Physics, Chemistry and Biology (IFM), Linköping University, Linköping SE-58183, Sweden
[c] School of Advanced Materials Science and Engineering, Sungkyunkwan University (SKKU), Suwon, 16419 Republic of Korea
E-mail: shenxinyu93@gmail.com， brlee@skku.edu
[d] Clarendon Laboratory, Department of Physics, University of Oxford, Oxford, UK
[e] Department of Chemistry, Research Institute for Convergence of Basic Science, Research Institute for Natural Sciences, Hanyang University, Seoul 04763, Republic of Korea
[f] Department of Materials Science and Engineering, Seoul National University, Seoul 08826, Republic of Korea
[g] Pohang Accelerator Laboratory, POSTECH, Pohang 37673, Republic of Korea
Electronic Supplementary Information (ESI) available: [details of any supplementary information available should be included here]. See DOI: 10.1039/x0xx00000x

The TMFPPO was incorporated into the PVK layer to modulate the energy level and hole mobility of the HTL for quasi-2D blue PeLEDs. Consequently, the LED with blended PVK:TMFPPO (9:1) HTL presented a peak EQE of 7.23% at 477 nm, much higher than the 4.95% of the PVK device, benefiting from the barrier-free hole injection and balanced hole-electron mobility in the perovskite layer. Taking the advantages of a modulator with deep HOMO level and excellent hole mobility is expected to facilitate the development of blue PeLEDs.

Results and discussion

As depicted in Fig. 1a, the TMFPPO was synthesized by oxidizing the TMFPP with hydrogen peroxide (H_2O_2) and purified via chloroform extraction (for details, see Supporting Information),[47] where the phosphine oxide functional and F can be used to obtain deep HOMO level.[45, 48, 49] Fourier transform infrared (FTIR) spectroscopy was utilized to characterize the as-prepared product; the distinct absorption peak at 1174 cm^{-1} can that can be observed in the purple curve that can be assigned to the stretching vibration of the P=O indicating the successful synthesis of TMFPPO (Fig. 1b). Tauc plots and ultraviolet photoelectron spectroscopy (UPS) were subsequently measured to feature the optical bandgap and the energy level of TMFPPO (Fig. 1c).[13,50] The TMFPPO exhibits a wide bandgap of 4.38 eV, and a deep HOMO level of -6.46 eV. Further, we fabricated a hole-only device using TMFPPO, with the structure of ITO / PEDOT: PSS / TMFPPO / MoO_3 / aluminium (Al) (inset of Fig. 1d). Fig. 1d presents the current density-voltage (J-V) curve, from which the hole mobility can be estimated by space-charge-limited-current region (SCLC) with Mott-Gurney law , $J = 9\varepsilon\varepsilon_0\mu V^2/(8L^3)$, where μ, J, ε, ε_0, V and L are the hole mobility, current density, relative dielectric constant, vacuum permittivity, applied voltage and the thickness of HTL, respectively.[51] By assuming that ε = 3.5,[51] the calculated hole mobility of TMFPPO is 1.26 × 10^{-4} $cm^2/(V{\cdot}s)$, as shown in Table S1. In addition, the holes can be injected favourably from the PEDOT:PSS to HTL with the deep LUMO level, implying that PEDOT:PSS works as a modification layer to promote carrier injection from ITO to HTL.

As discussed above, TMFPPO is a good candidate to regulate the energy level and hole mobility of PVK. TMFPPO and PVK were therefore solvated individually in chlorobenzene, blended at various ratios and deposited on the PEDOT: PSS film *via* spin-coating process. As the J-V curve of hole-only device displayed in the Figure S1, the calculated hole mobility of PVK, PVK:TMFPPO (9:1) and PVK:TMFPPO (7:3) is 1.04×10^{-5}, 1.84×10^{-5}, and 2.73×10^{-5} $cm^2/(V{\cdot}s)$, respectively. The hole mobility was improved obviously with the incorporation of TMFPPO. Although there is no obvious difference between the optical bandgaps of different blended HTLs (Fig. 2a, Fig. S2 and Table S2), the HOMO level of blended HTLs can be modulated continuously through manipulating the PVK:TMFPPO ratio, benefiting from the differences in HOMO levels (Fig. 2b and c). As seen in the UPS spectrum in Fig. 2b, the HOMO energy level of pristine PVK was determined to be -5.83 eV, while the blended HTLs exhibited HOMO levels of -6.19 eV (9:1) and -6.36 eV (7:3), respectively (Fig. 2c). Moreover, the charge injection in quasi-2D LEDs was investigated by analysing the J-V curves of hole-only and electron-only devices with $CsPbBr_3$: PEACl: YCl_3 as EML. The current density increased notably with increasing TMFPPO ratio, implying an enhanced hole injection efficiency (Fig. 2d). In particular, the J-V curve of the hole-only device incorporating a PVK:TMFPPO ratio of 9:1 exhibited a close resemblance to that of the electron-only device when the voltage is higher than 3V (Fig. 2e). Notably, the hole-only device with PVK:TMFPPO ratio of 7:3 displayed considerably higher current density compared to that of electron-only device. Meanwhile, by adding more TMFFPO into the PVK host, hole injection current can be further enhanced, but it is suspected of a slight mismatch between electrons and holes injection.

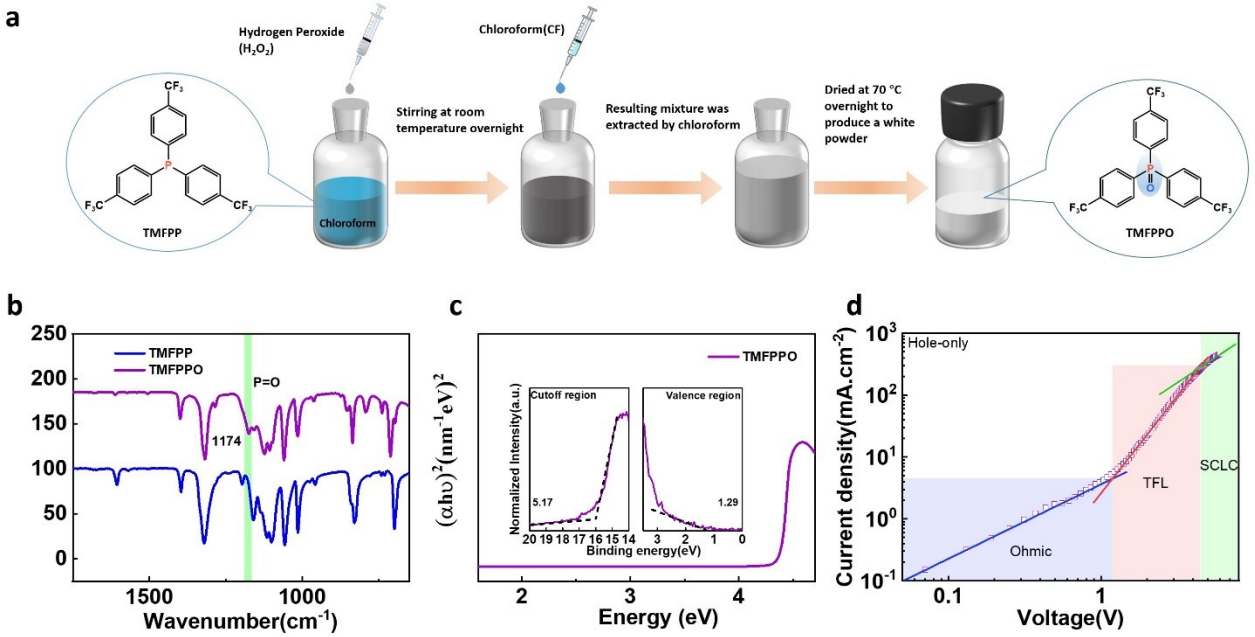

Fig. 1 (a) The synthesis process of TMFPPO, (b) FTIR of TMFPP and TMFPPO, (c) UPS and Absorption of TMFPPO, (d) J-V curve of holy-only device based on TMFPPO.

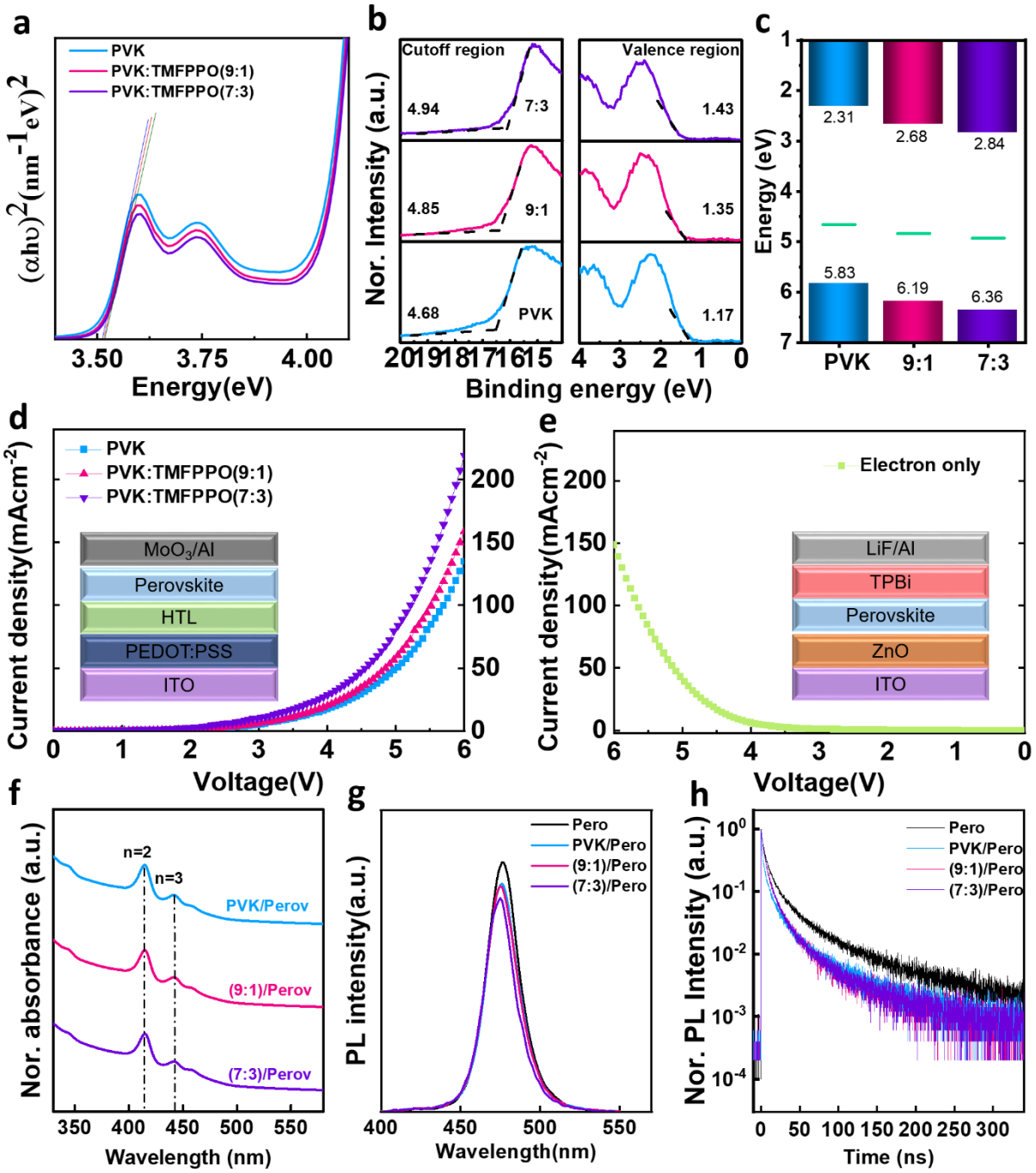

Fig. 2 (a) Absorption of films with various HTLs (b) UPS of different HTLs, (c) Energy diagrams of different HTLs, (d) The J-V curves of hole-only devices with the structure: ITO / PEDOT:PSS / blended HTLs / $CsPbBr_3$:PEACl:YCl_3 / MoO_3 / Al. (e) J-V curve of a hole-only device with the structure: ITO / ZnO / PEI / $CsPbBr_3$:PEACl:YCl_3 / 2,2',2''-(1,3,5-Benzinetriyl)-tris(1-phenyl-1-H-benzimidazole) (TPBi) / LiF / Al. (f) Absorption spectra, (g) PL spectra, and (h) PL decay lifetime of quasi-2D perovskite film without and with different HTLs.

The impact of different HTLs on the perovskite photo properties is depicted in Fig. 2f-h. As the UV-visible spectra shown in Fig. 2f, all perovskite films exhibited similar absorption peaks at 414 nm and 441 nm, corresponding to perovskite with n = 2 and n = 3, respectively, suggesting that the incorporation of TMFPPO does not exert a significant influence on the phase distribution of quasi-2D perovskite on different HTLs. Meanwhile, the PL spectra of perovskite films on bare glass and different HTLs are shown in Fig. 2g. No obvious peak shift occurs in PL emission of perovskite with different bottom layers, while the PL intensity is reduced with an increase in the TMFPPO ratio, which can be attributed to the carrier transfer from EML to HTL caused by the reduction in the energy barrier between the two layers.[10] Correspondingly, Fig. 2h exhibits the results of time-correlated single photon counting measurements (TCSPC) for these samples, and the average PL lifetimes (τ_{avg}) were determined through exponential decay fitting,[52] the τ_{avg} of perovskite on bare glass and PVK, 9:1, and 7:3 samples are 34.45, 20.05, 18.64, and 18.59 ns, respectively (Table S3), which aligns well with the

reduced PL intensity (Fig. 2e). As shown in Figure 2g, compared with the Perovskite deposited on the bare glass, the PL intensity of perovskite decreased obviously due to the carrier transfer at the HTL/EML interface.[53] There is negligible PL intensity between the Perovskite deposited on the PVK and PVK: TMFPPO (9:1), while decreased obviously when the TMFPPO ratio is increasing continuously, indicating that the amount of TMPPO should be rationally incorporated to prevent strong PL quenching at the HTL/EML interface.

Subsequently, the atomic force microscopy (AFM) images of different HTL films were examined to investigate the impact of incorporating TMFPPO into PVK on the film morphology. The root mean square (RMS) roughness varies from pristine PVK film (0.695 nm) to 9:1 (0.703nm) and 7:3 (0.711nm) (Fig. 3a-c). The increase in surface roughness contributes to a larger effective surface area available for the deposition of the subsequent layer.[54, 55] In addition, the water contact angles of PVK, PVK:TMFPPO (9:1), and PVK:TMFPPO (7:3) were measured as 84.8°, 82.5° and 80.9°, respectively, which is beneficial for the coverage of the blended HTL by the perovskite precursor solution owing to the increased surface energy (inset of Fig. 3a-c and Fig. S3).[56] Moreover, top-view SEM images in Fig. 3d-f display the perovskite films deposited on PVK:TMFPPO films with various TMFPPO ratios. There are no obvious differences between the perovskite films on the PVK and PVK:TMFPPO (9:1) films, while the one deposited on the PVK:TMFPPO (7:3) presented significant morphological imperfections characterized by generous voids and pinholes. It is postulated that the impaired film feature of the small molecular material TMFPPO hinders the formation of a homogeneous and continuous film, resulting in the aforementioned effect in the deposited perovskite film.[57] The crystal structure of the perovskite films on different HTLs was thoroughly examined by X-ray diffraction (XRD) (Fig. S4) and grazing-incidence wide-angle X-ray scattering (GIWAXS) (Fig. 3g-i). All the perovskite films present similar characteristic peaks, indicating similar quasi-2D perovskite crystal formed on various HTLs. Moreover, the Debye–Scherrer rings at q = 1.05, 1.51, 2.11 $Å^{-1}$ can be assigned to the crystallographic planes (100), (110), and (200) of the high-n phase, respectively. The rings in Fig. 3h and 3i exhibit higher intensity than those in Fig. 3g, i.e., the perovskite films are more random. As shown in Figure 3g-i, the circular Debye-Scherrer pattern gradually increases, indicating that the random orientation of crystals is strengthened compared to the parallel orientation. In this case, the charge transport in quasi-2D perovskite films can be improved through enhancing the contact between neighboring perovskite crystals with the introduction of TMFPPO to PVK.[8,58]

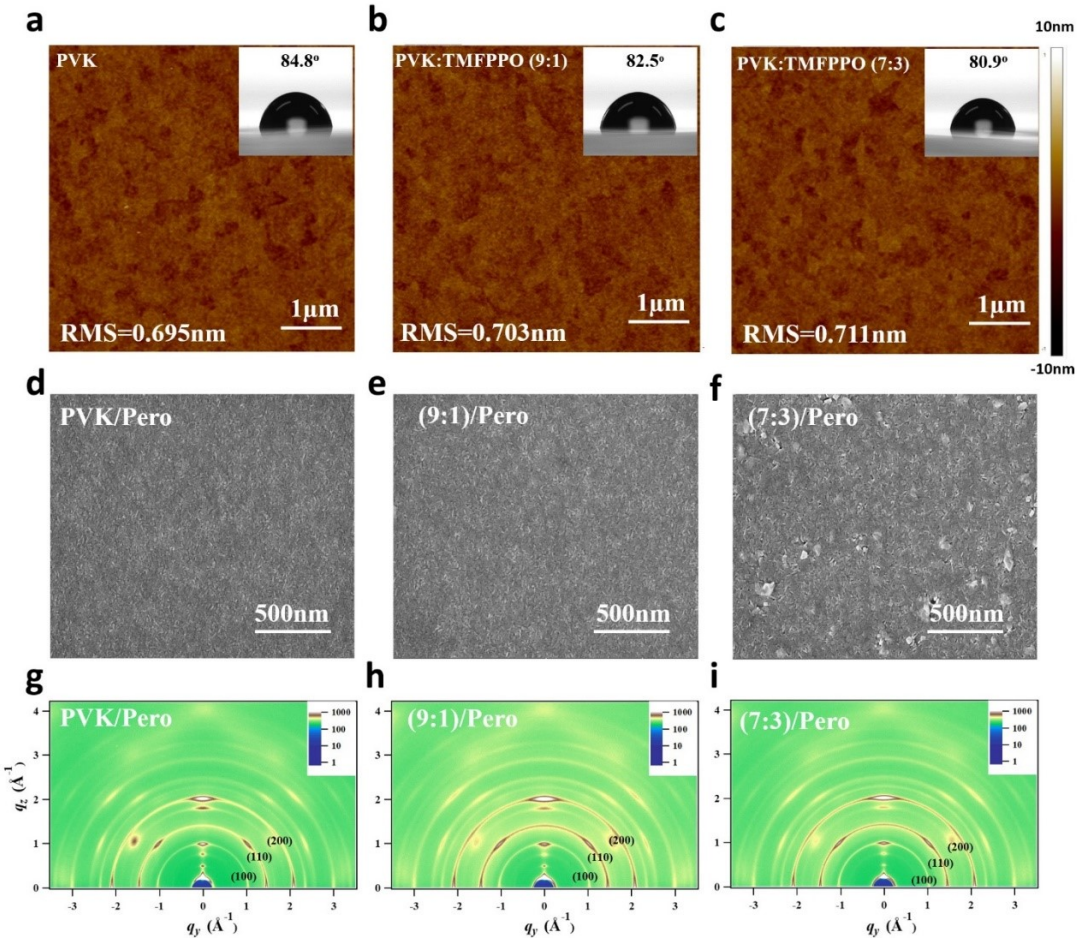

Fig. 3 (a–c) AFM images and contact angle measurements of various HTL films, (d–f) SEM images of the quasi-2D perovskite film deposited on various HTLs and (g–i) GIWAXS patterns of the quasi-2D perovskite films on different HTLs.

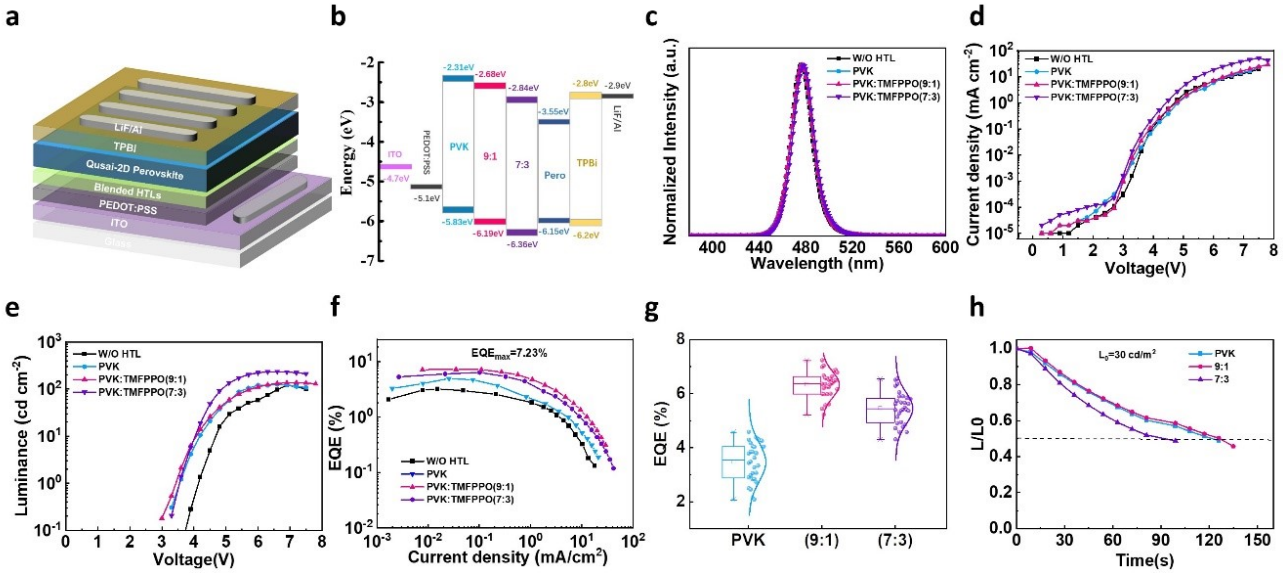

Fig. 4 (a) Device configuration, (b) Energy level diagram of a PeLED device, (c) Normalized electroluminescence (EL) spectra, (d) Current density-voltage (J-V) curves, (e) Luminance-voltage (L-V) curves and (f) EQE-voltage (EQE-V) curves, (g) Histogram for the maximum EQE of devices based on various HTLs, (h) Operational stability test of the optimal PeLED.

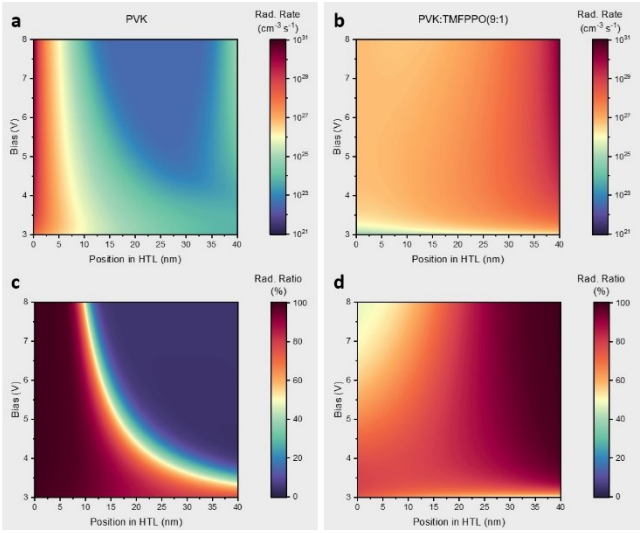

Fig. 5 Carrier Dynamics in the Device. (a) and (b) are the bias-dependent spatial profile of radiative recombination in the perovskite layer. (c) and (d) are the ratio of radiative recombination in the perovskite layer at different position and different biases.

Based on the previous analysis, we constructed perovskite LEDs with a device structure: ITO / PEDOT:PSS / Blended HTLs / quasi-2D perovskite / TPBi / LiF / Al (Fig. 4a), In this configuration, TPBi serves the dual purpose of an electron transport layer (ETL) and a hole blocking layer (EBL), LiF plays the role of the electron injection layer (EIL), and Al is functions as the cathode. The energy level diagram in Fig. 4b reveals that the hole injection barrier from the HTL to EML can be eliminated when the TMFPPO ratio is over 10%. The performance of the devices employing different HTLs is shown in Fig. 4c–h and Table 1. As shown in Fig. 4c, almost all LEDs exhibit a peak centered at 477 nm and a full-width at half maximum (FWHM) of 21 nm, which is consistent with their PL spectra in Fig. 2g. The current intensities of LEDs with blended HTLs are higher than that of the PVK device, demonstrating that carrier injection is improved by the blended HTL (Fig. 4d). The turn-on voltage decreases in the blended device benefiting from the enhanced and balanced carrier injection (Fig. 4e). The LED with 7:3 PVK:TMFPPO ratio presents a peak luminance of 234 cd m^{-2} at 6.6V, which correlates to the high current density. According to the EQE-J curve in Fig. 4f, the device with PVK:TMFPPO (9:1) achieves the highest EQE of 7.23%, presenting enhancements of 105% and 46% over the device without an HTL (maximum EQE of 3.52%) and the PVK-only LED (maximum EQE of 4.95%), respectively. The EQE decreases to 6.37% when the PVK:TMFPPO ratio is 7:3 in the blended HTL. This reduction in the device efficiency can be attributed to the exacerbated emission quenching at the interface, which is confirmed by the PL intensities and lifetimes in Fig. 2g and 2h.[59] As shown in Fig. 4g, the average EQEs for the PVK, 9:1, and 7:3 based LEDs are 3.3 ± 1.27%, 6.33 ± 0.9%, and 5.55 ± 0.99%, respectively, and therefore the devices exhibit good reproducibility. In this case, the operational stability of different devices was examined at the same initial luminance of 30 cd m^{-2} (Fig. 4h and Table S4). The LEDs with PVK, 9:1, and 7:3 exhibited operational lifetimes of 117, 126, and 99 seconds, respectively, demonstrating that the operational stability of the device can be prolonged with the energy level and hole mobility of HTL with the modulation of TMFPPO. In addition, we summarized recent reports on blue (~480nm) quasi-2D emissive parameters and present them in Table S5.

To further understand the influence of carrier injection on devices, a theoretical analysis has been conducted to investigate the carrier dynamics during device operation. The device structure in the model was simplified as Anode / HTL / Perovskite / TPBi / Cathode and the parameters used for simulations are listed in Table S6. Fig. 5a and b show simulated bias-dependent spatial profiles of radiative recombination for devices with HTLs of pure PVK and PVK:TMFPPO (9:1), respectively, while the corresponding ratios of radiative recombination rates among all the recombination channels are presented in Fig. 5c and d. As the HOMO level becomes lower, the distribution of radiative recombination is largely extended from the HTL/Perovskite interface to the overall layer. As shown in Fig. S5, the TMFPPO-induced HOMO modification boosts hole injection and increases the hole concentration in the emissive layer, compared with the hole accumulation in the HTL due to the injection barrier in pristine devices. Furthermore, as hole injection is improved, it facilitates the efficient radiative relaxation of carriers. This dramatic difference can be seen in Fig. 5c and d. Unlike the near-unity ratio of radiative recombination using blended HTL, PVK leads to serious non-radiative recombination in the device owing to the weak supplement of holes during operation. This deterioration caused by carrier imbalance becomes increasingly serious at high bias causing a severe drop in device efficiency, which is also verified in the EQE performance.

Table 1 Summary of blue quasi-2D PeLEDs device performances with different HTLs

Blended HTL	L_{max} [cd/m^2]	EQE_{max} [%]	Turn-on Voltage [V] @ 1 cd/m^2	Wavelength [nm]	FWHM [nm]
W/O	120	3.52	3.9	477	20
PVK	125	4.95	3.3	477	21
PVK:TMFPPO (9:1)	136	7.23	3.0	477	21
PVK:TMFPPO (7:3)	234	6.37	3.0	478	21

Conclusions

In summary, we developed the TMFPPO by the facile oxidation synthesis strategy, whose HOMO level and hole mobility are -6.46 eV and 1.26 × 10^{-4} cm^2/(V·s), respectively. TMFPPO was then incorporated into the PVK at specific ratios to modulate the energy level and hole mobility, giving rise to a barrier-free injection from the HTL to the EML. As a result, the LED with a PVK:TMFPPO ratio of 9:1 showed a peak EQE of 7.23%, representing a significant improvement over the devices without an HTL and pristine PVK-based devices. These findings provide insight into the optimization of HTLs for high-performance quasi-2D perovskite LEDs.

Author Contributions

X.F and X.S. designed the project and synthesized TMFPPO. X.F. conducted device fabrications and general characterizations. Y.W. contributed to simulation data calculations under the supervision of F.G. Y.Z., W.H.J. helped measured UPS. J.W.J., Y.G.K., S.J.W., H.S.C, T.W.L., S.H.P. and B.R.L. analysed the characterization of the materials and the LEDs. B.R.L. supervised the project. X.F. curated data and wrote the manuscript. X.S. and B.R.L. revised and prepared the manuscript.

Conflicts of interest

There are no conflicts to declare.

Acknowledgements

This work was supported by the National Research Foundation of Korea (NRF-2022H1D3A3A01077343, 2022R1A2C4002248, 2021M3H4A1A02049006 and 2021R1C1C1010266). This research was supported by the core research institute (CRI) program, the basic science research program through the national research foundation of Korea (NRF) under program number (2022R1A6A1A03051158).
This work was supported by the Samsung Research Funding & Incubation Centre of Samsung Electronics under Project Number SRFC-TC2103-04. This work has received funding from the European Union's Horizon 2020 research and innovation programme under the Marie Skłodowska-Curie grant agreement No 956270. The computations were enabled by resources provided by the National Supercomputer Centre (NSC), funded by Linköping University.

Notes and references

1. X. Shen, K. Kang, Z. Yu, W. H. Jeong, H. Choi, S. H. Park, S. D. Stranks, H. J. Snaith, R. H. Friend and B. R. Lee, *Joule*, 2023, **7**, 272-308.
2. L. Zhang, S. Hu, M. Guo, Y. Ren, L. Wei, W. Li, F. Lin, Z. Yang, Z. Yang, C. Liu and B. Liu, *Adv. Mater*., 2302059.
3. Z. Guo, Y. Liang, D. Ni, L. Li, S. Liu, Y. Zhang, Q. Chen, Q. Zhang, Q. Wang and H. Zhou, *Adv. Mater.*, 2302711.
4. D. Yang, B. Zhao, T. Yang, R. Lai, D. Lan, R. H. Friend and D. J. Di, *Adv. Funct. Mater.*, 2022, **32**, 2109495.

5. Y. Xu, L. Zhai, L. Sun, J. Wang, X. Tan, H. Huang, Y. Wang, G. Yang, K. Jiang and Y. Yang, *Chemical Communications,* 2022, **58**, 7132-7135.
6. Z. Guo, Y. Zhang, B. Wang, L. Wang, N. Zhou, Z. Qiu, N. Li, Y. Chen, C. Zhu and H. J. Xie, *Adv. Mater.*, 2021, **33**, 2102246.
7. W. H. Jeong, Z. Yu, L. Gregori, J. Yang, S. R. Ha, J. W. Jang, H. Song, J. H. Park, E. D. Jung and M. H. Song, *J. Mater. Chem. A*, 2021, **9**, 26750-26757.
8. Y. Liu, Z. Yu, S. Chen, J. H. Park, E. D. Jung, S. Lee, K. Kang, S.-J. Ko, J. Lim and M. H. Song, *Nano Energy*, 2021, **80**, 105511.
9. X. Shen, K. Kang, Z. Yu, W. H. Jeong, H. Choi, S. H. Park, S. D. Stranks, H. J. Snaith, R. H. Friend and B. R. Lee, *Joule*, 2023, **7**, 272-308.
10. Z. Yu, W. H. Jeong, K. Kang, H. Song, X. Shen, H. Ahn, S. W. Lee, X. Fan, J. W. Jang and S. R. Ha, *J. Mater. Chem. A*, 2022, **10**, 13928-13935.
11. C. Zhao, W. Wu, H. Zhan, W. Yuan, H. Li, D. Zhang, D. Wang, Y. Cheng, S. Shao and C. J. Qin, *Angew. Chem. Int. Ed.*, 2022, **61**, e202117374.
12. G. Yang, X. Tan, L. Zhai, H. Huang, Y. Wang, K. Jiang, Y. Yang, L. Zhang, Z. a. Tan and H. Wen, *Chem. Commun.,* 2023, **59**, 5906-5909.
13. J. S. Kim, J.-M. Heo, G.-S. Park, S.-J. Woo, C. Cho, H. J. Yun, D.-H. Kim, J. Park, S.-C. Lee and S.H. Park, *Nature* 2022, **1-7**.
14. Z. Liu, W. Qiu, X. Peng, G. Sun, X. Liu, D. Liu, Z. Li, F. He, C. Shen and Q. J. Gu, *Adv. Mater.*, 2021, **33**, 2103268.
15. M. Xie, J. Guo, X. Zhang, C. Bi, L. Zhang, Z. Chu, W. Zheng, J. You and J. J. Tian, *Nano Lett.*, 2022, **22**, 8266-8273.
16. L. Zhang, N. Li, D. Liu, G. Tao, W. Xu, M. Li, Y. Chu, C. Cao, F. Lu and C. J. Hao, *Angew. Chem. Int. Ed.*, 2022, **61**, e202209337.
17. L. Zhu, H. Cao, C. Xue, H. Zhang, M. Qin, J. Wang, K. Wen, Z. Fu, T. Jiang and L. J. Xu, *Nature Communications,* 2021, **12**, 5081.
18. Y. Hassan, J. H. Park, M. L. Crawford, A. Sadhanala, J. Lee, J. C. Sadighian, E. Mosconi, R. Shivanna, E. Radicchi and M. J. Jeong, *Nature*, 2021, **591**, 72-77.
19. W. Bai, T. Xuan, H. Zhao, H. Dong, X. Cheng, L. Wang and R.-J. Xie, *Adv. Mater.*, 2023, 2302283.
20. Y. Shen, Y. Q. Li, K. Zhang, L. J. Zhang, F. M. Xie, L. Chen, X. Y. Cai, Y. Lu, H. Ren and X. J. Gao, *Adv. Funct. Mater.*, 2022, **32**, 2206574.
21. C. Wang, D. Han, J. Wang, Y. Yang, X. Liu, S. Huang, X. Zhang, S. Chang, K. Wu and H. J. N. C. Zhong, *Nature Communications*, 2020, **11**, 6428.
22. Q. Wang, X. Wang, Z. Yang, N. Zhou, Y. Deng, J. Zhao, X. Xiao, P. Rudd, A. Moran and Y. J. Yan, *Nature Communications*, 2019, **10**, 5633.
23. Y. Dong, Y.-K. Wang, F. Yuan, A. Johnston, Y. Liu, D. Ma, M.-J. Choi, B. Chen, M. Chekini and S.-W. J. Baek, *Nature Nanotech.*, 2020, **15**, 668-674.
24. X. Peng, C. Yan, F. Chun, W. Li, X. Fu, W. J. Yang *J. Alloys Compd.*, 2021, **883**, 160727.
25. Z. Li, Z. Chen, Y. Yang, Q. Xue, H.-L. Yip and Y. J. Cao, *Nature Communications*, 2019, **10**, 1027.
26. X. Zheng, S. Yuan, J. Liu, J. Yin, F. Yuan, W.-S. Shen, K. Yao, M. Wei, C. Zhou and K. J. Song, *ACS Energy Lett.*, 2020, **5**, 793-798.
27. F. Wang, Z. Wang, W. Sun, Z. Wang, Y. Bai, T. Hayat, A. Alsaedi and Z. S. Tan, *Small,* 2020, 16, 2002940.
28. S. Yuan, T. Fang, J. Huang, X. Li, C. Wei, Y. Zhou, Y. Li, X. Zheng, J. Huang and J. J. Su, *ACS Energy Lett.*, 2023, **8**, 818-826.
29. A. Fakharuddin, W. Qiu, G. Croes, A. Devižis, R. Gegevičius, A. Vakhnin, C. Rolin, J. Genoe, R. Gehlhaar and A. J. Kadashchuk, *Adv. Funct. Mater.*, 2019, **29**, 1904101.
30. A. Liu, C. Bi, R. Guo, M. Zhang, X. Qu and J. J. Tian, *Adv. Opt. Mater.*, 2021, **9**, 2002167.
31. X. Zhang, H. Dai, J. Zhao, S. Wang and X. J. Sun, *Thin Solid Films*, 2016, **603**, 187-192.
32. L. Zhang, C. Sun, T. He, Y. Jiang, J. Wei, Y. Huang, M. J. Yuan, *Light Sci. Appl.*, 2021, **10**, 61.
33. L. Wang, Z. Shi, Z. Ma, D. Yang, F. Zhang, X. Ji, M. Wang, X. Chen, G. Na and S. J. Chen, *Nano Lett.*, 2020, **20**, 3568-3576.
34. Y. Liu, J. Cui, K. Du, H. Tian, Z. He, Q. Zhou, Z. Yang, Y. Deng, D. Chen and X. J. Zuo, *Nature Photonics*, 2019, **13**, 760-764.
35. Y. Jiang, M. Cui, S. Li, C. Sun, Y. Huang, J. Wei, L. Zhang, M. Lv, C. Qin and Y. J. Liu, *Nature Communications*, 2021, **12**, 336.
36. Z. Ren, X. Xiao, R. Ma, H. Lin, K. Wang, X. W. Sun and W. C. H. Choy, *Adv. Funct. Mater*., 2019, **29**, 1905339.
37. Y. Nah, D. Solanki, Y. Dong, J. A. Röhr, A. D. Taylor, S. Hu, E. H. Sargent and D. H. Kim, *Adv. Sci.*, 2022, **9**, 2201807.
38. D. Ma, P. Todorović, S. Meshkat, M. I. Saidaminov, Y.-K. Wang, B. Chen, P. Li, B. Scheffel, R. Quintero-Bermudez, J. Z. Fan, Y. Dong, B. Sun, C. Xu, C. Zhou, Y. Hou, X. Li, Y. Kang, O. Voznyy, Z.-H. Lu, D. Ban and E. H. Sargent, *J. Am. Chem. Soc*., 2020, **142**, 5126-5134.
39. Y. S. Shin, C. B. Park, A. Adhikari, Y. J. Yoon, H. W. Cho, J. G. Son, J. Seo, T. Song, W. Lee, J. Yeop, J. W. Kim, M. Gong, B. Walker, O.-H. Kwon, G.-H. Kim and J. Y. Kim, *ACS Energy Lett.*, 2022, **7**, 3345-3352.
40. Z. Yu, W. H. Jeong, K. Kang, H. Song, X. Shen, H. Ahn, S. W. Lee, X. Fan, J. W. Jang, S. R. Ha, J. W. Min, J. H. Park, J. Han, E. D. Jung, M. H. Song, D. W. Chang, W. B. Im, S. H. Park, H. Choi and B. R. Lee, *J. Mater. Chem. A*, 2022, **10**, 13928-13935.
41. O. Y. Kim and J. Y. Lee, *Journal of Industrial and Engineering Chemistry*, 2012, **18**, 1029-1032.
42. S. Gong, Y.-L. Chang, K. Wu, R. White, Z.-H. Lu, D. Song and C. Yang, *Chemistry of Materials*, 2014, **26**, 1463-1470.
43. S. O. Jeon, K. S. Yook, C. W. Joo and J. Y. Lee, *Adv. Mater.*, 2010, **22**, 1872-1876.
44. S. Shao, J. Ding, L. Wang, X. Jing and F. Wang, *Journal of the American Chemical Society*, 2012, **134**, 15189-15192.
45. E. He, Z. Zheng, Y. Lu, F. Guo, S. Gao, X. Pang, G. T. Mola, L. Zhao and Y. J. Zhang, *J. Mater. Chem. A*, 2020, **8**, 11381-11390.
46. G. P. Kini, Y. W. Han, S. J. Jeon, Y. J. Lee and D. K. J. Moon, *Mater. Chem. Front*., 2022, **6**, 1759-1769.
47. D. Ma, K. Lin, Y. Dong, H. Choubisa, A. H. Proppe, D. Wu, Y.-K. Wang, B. Chen, P. Li, J. Z. Fan, F. Yuan, A. Johnston, Y. Liu, Y. Kang, Z.-H. Lu, Z. Wei and E. H. Sargent, *Nature*, 2021, **599**, 594-598.
48. O. Y. Kim, J. Y. Lee, J*ournal of Industrial and Engineering Chemistry*, 2012, **18**, 1029-1032.
49. D. Kim, L. Zhu and J.-L. J. Bredas, *Chem. Mater.*, 2012, **24**, 2604-2610.
50. Q. Tan, Z. Li, G. Luo, X. Zhang, B. Che, G. Chen, H. Gao, D. He, G. Ma and J. J. Wang, *Nature* 2023, 1-3
51. X. Shen, H. Wu, X. Zhang, M. Xu, J. Hu, J. Zhu, B. Dong, W. W. Yu and X. Bai, *J. Phys. Chem. Lett.*, 2021, **12**, 94-100.
52. J. Byun, H. Cho, C. Wolf, M. Jang, A. Sadhanala, R. H. Friend, H. Yang and T. W. Lee, *Adv. Mater.*, 2016, **28**, 7515-7520.
53. B. R. Lee, J. C. Yu, J. H. Park, S. Lee, C.-K. Mai, B. Zhao, M. S. Wong, E. D. Jung, Y. S. Nam, S. Y. Park, D. Di Nuzzo, J. Y. Kim, S. D. Stranks, G. C. Bazan, H. Choi, M. H. Song and R. H. Friend, *ACS Nano*, 2018, **12**, 5826-5833.
54. H. J. An, S. D. Baek, D. H. Kim and J. M. Myoung, *Adv. Funct. Mater.*, 2022, **32**, 2112849.
55. C. Li, J. Zhang, J. Han and B. Yao, *Sci. Rep.*, 2021.

56. W. Li, H. Dong, X. Guo, N. Li, J. Li, G. Niu and L. J. Wang, *J. Mater. Chem. A*, 2014, **2**, 20105-20111.
57. L. Duan, L. Hou, T.-W. Lee, J. Qiao, D. Zhang, G. Dong, L. Wang and Y. J. Qiu, *J. Mater. Chem*., 2010, **20**, 6392-6407.
58. H. D. Lee, H. Kim, H. Cho, W. Cha, Y. Hong, Y. H. Kim, A. Sadhanala, V. Venugopalan, J. S. Kim , J. W. Choi, C. L. Kim, D. Kim, H. Yang, R. H. Friend and T. W. Lee, *Adv. Funct. Mater.*,2019, **29**, 1901225.
59. J. Lu, X. Guan, Y. Li, K. Lin, W. Feng, Y. Zhao, C. Yan, M. Li, Y. Shen and X. J. Qin, *Adv. Mater.*, 2021, **33**, 2104414.

